ACS OMEGA

http://pubs.acs.org/journal/acsodf

Article

# Theoretical Modeling of the Impact of Salt Precipitation on $CO_2$ Storage Potential in Fractured Saline Reservoirs

Yen A. Sokama-Neuyam,* Patrick Boakye, Wilberforce N. Aggrey, Nicholas O. Obeng, Francis Adu-Boahene, Seung Han Woo, and Jann Rune Ursin

Cite This: *ACS Omega* 2020, 5, 14776−14785

Read Online

ACCESS | Metrics & More | Article Recommendations

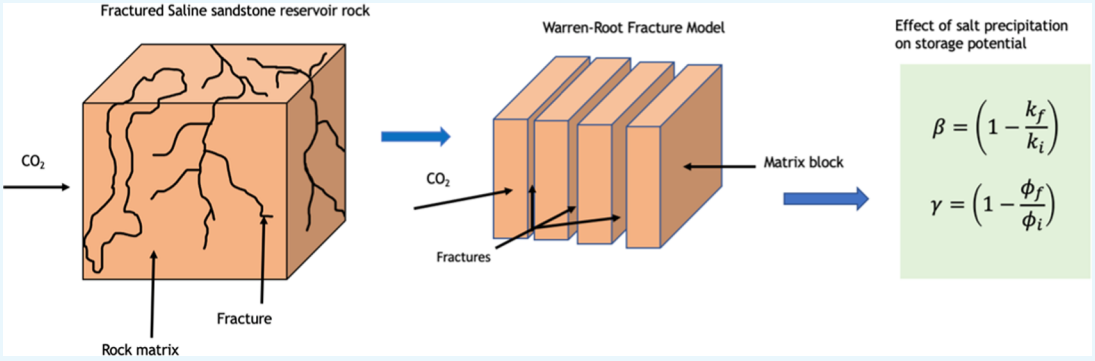


**ABSTRACT:** Deep saline reservoirs have the capacity to hold large volumes of $CO_2$. However, apart from the high brine salinity, which poses an injectivity challenge, a high percentage of saline reservoirs are also fractured. The mechanisms of drying and salt precipitation and the resulting impact on $CO_2$ injection are unique in fractured reservoirs. Analytical models were developed to investigate the impact of salt precipitation on $CO_2$ injectivity and storage capacity. Two types of fractured saline reservoirs were considered: type I fractured reservoirs, where storage capacity and injectivity are contributed by only fractures, and type II fractured reservoirs, where both fractures and the adjacent rock matrix blocks contribute to $CO_2$ storage and injectivity. We found that, depending on the initial brine salinity, salt precipitation could severely impair $CO_2$ injectivity and reduce storage capacity. Salt precipitation had a fourfold impact on $CO_2$ injectivity compared to storage capacity. Type I reservoirs with high irreducible brine saturation were less susceptible to salt clogging in the fractures. The results also suggest that fractures with rectangular aperture were less likely to be plugged by salt compared to elliptical fractures. Contrary to previous reports, some fractured deep saline reservoirs may not be suitable for $CO_2$ storage. Generally, type II fractured reservoirs were found to be more suitable for $CO_2$ storage in terms of susceptibility to salt clogging. The findings provide valuable understanding of the mechanisms and effect of drying and salt precipitation on $CO_2$ storage potential, making a strong case for $CO_2$ storage in naturally fractured deep saline reservoirs.

## 1. INTRODUCTION

According to the IEA Global Energy and $CO_2$ Status Report, about 33.1 Gt $CO_2$ was emitted from energy-related sources in 2018, representing an about 1.7% rise in global $CO_2$ emission.[1] A pragmatic $CO_2$ emission reduction plan is required to reduce the amount of $CO_2$ emitted into the environment and sustain fossil-related energy production. $CO_2$ capture, utilization, and storage (CCUS) is a technically feasible option to achieve carbon neutrality by 2050. Storage capacity and well injectivity determine the storage potential of a CCUS project.[2] $CO_2$ sequestration through enhanced oil recovery (EOR) in existing reservoirs and storage in depleted oil and gas reservoirs are currently the most economically attractive options.[3−7] $CO_2$ storage in geothermal reservoirs have also been considered.[8−10] But deep saline aquifers have the highest potential in terms of volume available to hold $CO_2$.[11,1211,12] Preliminary works have shown that naturally fractured deep saline reservoirs could be useful for $CO_2$ storage.[13] However, drying and salt precipitation at the injection inlet could reduce $CO_2$ storage potential.[14−16] The mechanisms of salt precipitation in naturally fractured saline formations and the impact of salt deposition on $CO_2$ storage potential are still not well understood.

When $CO_2$ is injected into homogeneous saline sandstone rocks, water is removed through advection and vaporization. At

Received: April 13, 2020
Accepted: June 1, 2020
Published: June 15, 2020






https://dx.doi.org/10.1021/acsomega.0c01687
*ACS Omega* 2020, 5, 14776−14785

mobile brine saturation, brine is displaced immiscibly out of the rock. As the aqueous phase becomes immobile, water evaporates into the $CO_2$ stream.[17,18] Eventually, a dry-out zone is created around the injection inlet, where salt is precipitated into the pores.[19−21] The salt saturation gradient created across the drying front draws brine toward the dry-out zone through capillary backflow of brine.[14,18,22] The deposited salt in the dry-out zone then reduces the flow path of injected $CO_2$, consequently impairing injectivity.

Various results of flow impairment induced by salt precipitation have been reported. In experiments involving Berea sandstones, Muller et al.[23] reported about 60% reduction in absolute permeability and Wang et al.[24] found about 50% impairment in $CO_2$ relative permeability. In similar experiments, Tang et al.[25] reported about 14 and 83% reductions in porosity and absolute permeability, respectively. Porosity reduction of around 2−25% and permeability impairment between 13 and 75% have also been reported from experiments involving other porous materials.[16,26,27] Results reported from analytical and numerical simulations are consistent with most of the experimental findings.[20,28−30]

An important characteristic of fractured reservoir rocks is their dual-porosity systems, which consist of primary porosity formed by the pore spaces in the rock matrix and secondary porosity formed mainly by fractures and vugs.[31] In fractured reservoirs, storage capacity and permeability may be provided by either the fractures or by fractures and the rock matrix depending on the fracture density.[32] Under stabilized flow in a double-porosity system, fluid flows toward the well mainly through the low resistance fracture network, whereas the matrix blocks supply fluid to the surrounding fractures.

Oh et al.[33] conducted experimental and numerical studies to investigate the effect of fractures on the transport properties of $CO_2$ and storage capacity. They observed that at different injection rates, brine displacement in the fractures was different from displacement in the rock matrix. They found that while the fractured core had a twofold injectivity compared to homogeneous core, the storage capacity of the homogeneous core was about 1.5 times higher. They also reported evidence of salt precipitation in both cases of the experiments. Borgia et al.[9] investigated the mechanism of salt precipitation in fractured aquifer. They reported drying and salt precipitation close to the production well as the $CO_2$ plume develops. Tian et al.[34] studied the effect of mineral dissolution on rock porosity in fractured reservoirs through reactive transport modeling. They observed that the dissolution reaction increases with fracture width and the change in porosity is strongly dependent on $CO_2$ injection time. More recently, Rezk and Foroozesh[35] investigated the effect of fracture properties on the transport and storage of $CO_2$ in fractured heterogeneous saline reservoirs. $CO_2$ injection into fractured porous media for enhanced oil recovery (EOR), environmental impact analysis, and other effects have also been studied.[36,37]

Attempts have been made to unravel the mechanisms of salt deposition and permeability impairment in fractured deep saline reservoirs.[13,38,39] Ott et al.[13] conducted experimental studies to investigate the mechanisms of drying and salt precipitation in single-porosity sandstone and dual-porosity dolomite rocks. They found that, while effective permeability improved in the single-porosity sandstone, there was a strong impairment in the dolomite rock. They concluded that the extent of permeability impairment in fractured rocks depends on the ratio of the volume of secondary to primary porosity. Ott et al.[38] attempted to explain the mechanisms of salt precipitation in dual-porosity rocks through core-flood experiments coupled with micro-computerized tomography scanning. They observed that transport of salt between the micropores and the microporous subsystems determines the distribution of deposited salts in the pore space. March et al.[39] derived a new matrix-fracture fluid transfer function to study the effect of fractures on $CO_2$ storage potential and the maximum volumetric storage of the rock matrix in dual-porosity rocks. They found that a larger volume of the rock matrix is used for storage in deep saline reservoirs located in cold basins compared to shallow reservoirs in warm basins. However, the distribution of salt in the pores and the effect of salt precipitation on $CO_2$ injectivity in dual-porosity reservoir rocks have not been investigated.

The objective of this work is to quantify the effect of salt precipitation on $CO_2$ storage potential in dual-porosity rocks. Static analytical models will be developed to simulate the mechanisms and influence of salt precipitation on the $CO_2$ storage capacity and injectivity in fractured reservoirs. Two types of fractured reservoirs will be considered: type I fractured reservoirs, where secondary porosity contributes all of the $CO_2$ storage capacity and injectivity, and type II reservoirs, where storage capacity and injectivity are contributed by primary and secondary porosity. The effect of matrix residual brine saturation, fracture geometry, and initial brine salinity will be investigated.

This work is organized as follows. First, the modeling process is described and relevant equations and data are presented. The simulation process is then described and results are presented. The results are analyzed and discussed, and some practical implications are identified, leading to conclusions that provide useful insight into the quantitative effect of salt drop-out on $CO_2$ injection in fractured deep saline reservoirs. We show that $CO_2$ injection in fractured saline aquifers is feasible if the injection process is optimized to reduce salt deposition.

## 2. MODELING WORK

In this section, we derive a static analytical model from a modified Warren−Root framework to quantify the change in porosity and absolute permeability based on salt distribution at complete dry-out in fractured reservoir rock. The mechanisms of salt precipitation and distribution of precipitated salt in the fractures and rock matrix are modeled based on past experimental findings. Assumptions are also proposed, leading to a derivation of analytical models that demonstrate the fundamental mechanisms of $CO_2$ flow and salt deposition in dual-porosity reservoirs. The following are some of the main assumptions adopted in the modeling process:

1. A fully homogeneous saline reservoir rock containing fractures with smooth walls.
2. Negligible chemical interaction between the injection fluid and the contents of the reservoir rock.
3. The rock matrix and the fractures are fully filled with formation brine prior to $CO_2$ injection.
4. Drying and salt precipitation are severe around the wellbore injection region due to high fluxes.
5. The aqueous phase in the fractures along the flow direction is swept out during the advection stage.

The objective is to derive simple models that capture the basic mechanisms and are capable of providing acceptable estimates of the quantitative impact of salt deposition on $CO_2$ storage in fractured deep saline reservoirs.



https://dx.doi.org/10.1021/acsomega.0c01687
ACS Omega 2020, 5, 14776−14785

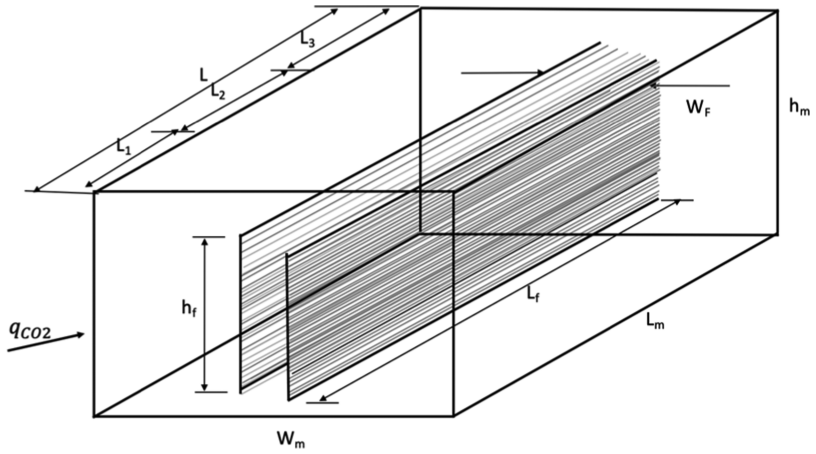


**Figure 1.** Schematics of the fractured reservoir rock model.

**2.1. Model Development.** A modified Warren−Root model consisting of a block of sandstone rock with length $L_m$, width $w_m$, and height $h_m$ containing $n$ rectangular-shaped fractures with varying widths $w_{f1}$, $w_{f2}$, $w_{f3}$, ..., $w_{fn}$ interspersed between slides of rock matrix was used (Figure 1). This is a one-dimensional (1D) model with an inlet at the wellbore and an outlet at a reservoir radius within the dry-out zone where salt is often precipitated during $CO_2$ injection. Hurter et al.[29] have reported from numerical simulations that the dry-out region could extend up to about 10 m within 2 years of $CO_2$ injection. Thus, the length of the reservoir block was selected within this high drying zone. Radial flow into the reservoir is of utmost importance because even in a highly heterogeneous reservoir, salt precipitation along the vertical permeability is very minimal compared to that along the horizontal direction where the fluxes are higher. Around the vicinity of the wellbore, flow into the reservoir can be adequately approximated with a 1D model as the ultimate interest is in the horizontal flow where salt precipitation has the highest effect on $CO_2$ injection. A two-dimensional (2D) or three-dimensional (3D) model can be used to extend the study to investigate the effect of reservoir heterogeneity on salt precipitation in the fractures. Thus, the current study assumes a homogeneous reservoir with maximum salt precipitation along the horizontal direction in the wellbore vicinity.

**2.2. Type I Fractured Reservoirs.** In this study, type I fractured reservoirs refer to reservoirs where storage capacity and injectivity are contributed by the secondary porosity or macropores. The injected $CO_2$ flows mainly through the fractures, with the adjacent matrix blocks supplying brine to the fractures.[13] The injected $CO_2$ does not invade the rock matrix due to the relatively low rock permeability. Rectangular fractures are considered to simplify the mechanism of salt distribution. Considering rectangular fractures with smooth walls, the initial absolute permeability of the rock can be derived from the Hagen−Poiseuille equation and Darcy's law as

$$k_i = \frac{\sum_{i=1}^{N} h_{fi} w_{fi}^3}{12A} \tag{1}$$

In eq 1, $h_{fi}$ and $w_{fi}$ are the height and aperture of fracture $i$, $A$ is the total flow area of the reservoir block, and $N$ is the total number of fractures in the block. Similarly, the initial total porosity of the rock is derived as

$$\phi_i = \frac{\sum_{i=1}^{N} h_{fi} w_{fi}}{A} \tag{2}$$

In eqs 1 and 2, we have assumed that the fractures run through the length of the block and thus $L_f = L_m$.

**2.3. Quantifying the Impact of Salt Precipitation.** The reservoir block is filled with brine prior to $CO_2$ injection. The injected supercritical $CO_2$ displaces brine in the fractures until all brine in the fractures break through at the reservoir outlet. Since the matrix blocks are not conductive, we assume that the displaced brine in the fractures does not invade the adjacent matrix blocks. Thus, the matrix blocks are still filled with brine since they have not been invaded by injected $CO_2$. A saturation gradient is established between the dry-out fractures and the brine-saturated rock matrix. This saturation gradient draws brine from the adjacent rock matrix into the fractures through capillary flow.[18,20] The high-flow-rate $CO_2$ in the fractures dries out the brine, precipitating salt in the fractures, beginning at the injection inlet where the fluxes are highest.[10]

Since drying commences at the injection inlet, the solid salt saturation will be higher around the injection inlet and decrease steadily across the length of the fracture due to capillary backflow of brine toward the injection inlet.[14,38,40] Assuming the rock matrix is fairly homogeneous and the fractures are fairly smooth, the thickness of the deposited salt will be practically the same on both sides of the fracture since the matrix blocks have the same volumetric capacity and conductance.

The completely dried rock is divided into three sections, $L_1$, $L_2$, and $L_3$, from the injection inlet along the length of the reservoir rock according to the mode of salt precipitation and the amount of salt expected to be deposited.[41] A dimensionless dry-out length, $l_{di}$, is defined to track the drying process

$$l_{di} = \frac{L_i}{L} \tag{3}$$

where $i$ = 1, 2, and 3 for $L_1$, $L_2$, and $L_3$, respectively. Assuming all mobile brine in the rock matrix will flow into the fractures for drying, the solid salt saturation, $S_{si}$, at each region $i$ of the block can be estimated from[41]


https://dx.doi.org/10.1021/acsomega.0c01687
ACS Omega 2020, 5, 14776−14785

$$S_s = \begin{cases} S_{s1} = \dfrac{\alpha S_l(1 - S_{wr})}{\rho_s}, & l_d \le l_{d1} \\ S_{s2} = S_{s1} + \dfrac{(S_{s3} - S_{s1})(l_{d2} - l_{d1})}{(l_{d3} - l_{d1})}, & l_{d1} < l_d \le l_{d2} \\ S_{s3} = \dfrac{S_l(1-S_{wr})}{\rho_s}, & l_d > l_{d2} \end{cases} \tag{4}$$

where $S_{wr}$ is immobile brine saturation in the rock matrix, $S_l$ is the salinity of brine in g/L, $\rho_s$ is the salt density in g/L, and $\alpha$ is a salt distribution factor. The deposited salt along the boundaries of the fractures reduces the width of the fracture $w_{fi}$ by $\Delta w_{fi}$, which can be quantified from mass balance and fractional flow[20,41]

$$\Delta w_{fi} = \frac{2}{3}\frac{S_{si} w_{fi}}{l_{di}} \tag{5}$$

The permeability of the impaired rock after salt precipitation can then be quantified as

$$k_f = \frac{\sum_{i=1}^{N} h_{fi}(w_f - \Delta w_f)_i^3}{12A} \tag{6}$$

Since $S_s$ changes along the rock according to eq 4, the reservoir block is modeled as three rock layers in series with varying permeabilities $k_1$, $k_2$, and $k_3$

$$k = \begin{cases} k_1, & l_d \le l_{d1} \\ k_2, & l_{d1} < l_d \le l_{d2} \\ k_3, & l_d > l_{d2} \end{cases} \tag{7}$$

After salt deposition, the impaired permeability of the layered rock is then calculated from

$$k_f = \frac{L}{L_1/k_1 + L_2/k_2 + L_3/k_3} \tag{8}$$

Similarly, the porosity of the rock after impairment is calculated from

$$\phi_f = \left( \left[ \sum_{i=1}^{N} h_{fi}(w_f - \Delta w_f)_i \right]_1 L_1 + \left[ \sum_{i=1}^{N} h_{fi}(w_f - \Delta w_f)_i \right]_2 L_2 + \left[ \sum_{i=1}^{N} h_{fi}(w_f - \Delta w_f)_i \right]_3 L_3 \right) / AL \tag{9}$$

We then derive simple dimensionless parameters $\beta$ and $\gamma$ to estimate the effect of salt impairment on injectivity and storage capacity, respectively

$$\beta = \left(1 - \frac{k_f}{k_i}\right) \tag{10}$$

$$\gamma = \left(1 - \frac{\phi_f}{\phi_i}\right) \tag{11}$$

where $\beta$ and $\gamma$ are expressed in percentages. These dimensionless parameters can be used to estimate the effect of precipitated salt on rock permeability and porosity.

**2.4. Impact of Fracture Geometry.** To study the effect of fracture geometry, elliptical-shaped fractures with the same volumetric capacity and orientation as the rectangular fractures were considered (Figure 2). The reservoir block is a type I fractured reservoir with the same dimensions as described in the previous section. From the Hagen−Poiseuille equation and Darcy's law, the absolute permeability and total porosity of the block can be derived as

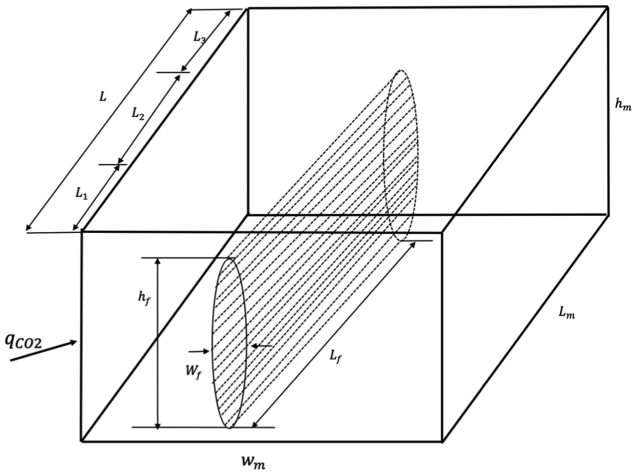


**Figure 2.** Schematics of the fractured reservoir rock containing elliptical fractures.

$$k = \frac{\pi}{64A} \sum_{i=1}^{N} \frac{h_f^3 w_f^3}{(h_f^2 + w_f^2)} \tag{12}$$

$$\phi = \frac{\pi}{4A} \sum_{i=1}^{N} w_{fi} h_{fi} \tag{13}$$

With some modifications, eqs 3−11 can be adapted to compute the change in storage potential of the impaired rock for elliptical fractures. The resulting permeability impairment and effect on volumetric capacity are then compared to the rectangular fractures.

**2.5. Type II Fractured Reservoirs.** In this work, type II reservoirs refer to fractured reservoirs where both the rock matrix and fractures contribute to fluid conductivity and $CO_2$ storage. The rock matrix blocks are fully conductive, and injected $CO_2$ flows through the fractures and the pore spaces within the rock. For fracture flow rate, $q_f$, and matrix flow rate, $q_m$, the total volumetric flow through the block is given by

$$q_t = q_m + q_f \tag{14}$$

A bundle of tubes model is used to quantify fluid conductivity in the micropores because salt deposition can be easily described by a reduction in the tubes flow area by deposited salts similar to the fracture network. If the matrix porosity is $\phi_m$ and the capillary tubes have equal radii, $r_c$, the total number of capillary tubes in the rock can be estimated from

$$n_c = \frac{\phi_m A_m}{\pi r_c^2} \tag{15}$$

where $A_m$ is the cross-sectional area of the reservoir block. From the Hagen−Poiseuille equation and Darcy's law, the total absolute rock permeability can be derived as


https://dx.doi.org/10.1021/acsomega.0c01687
ACS Omega 2020, 5, 14776−14785

$$k = \left[\frac{n_c \pi r_c^4}{8} + \frac{\sum_{i=1}^{N} h_{fi} w_{fi}^3}{12}\right] / A_t \quad (16)$$

In eq 16, we have assumed rectangular-shaped fractures and $A_t$ is the total cross-sectional area of the rock. Similarly, the total porosity is the sum of the matrix and fracture porosities, which can be expressed as

$$\phi = \frac{\sum_{i=1}^{N} h_{fi} w_{fi} + n_c \pi r_c^2}{A_t} \quad (17)$$

The mechanisms of drying and salt precipitation in type II reservoirs are different from those of type I reservoirs. We assume the reservoir rock is fully saturated with brine prior to $CO_2$ injection. The injected $CO_2$ invades the fractures first and then the matrix blocks, since the fractures offer the least flow resistance. We assume that all brine in the fractures will be advected during immiscible displacement. Ott et al.[13] reported from experimental studies that salt only precipitates significantly in the macropores. They observed that salt coming from the micropores are precipitated mainly in the macropores. Based on this finding, we assume that all mobile brine in the matrix blocks will be advected during immiscible displacement. The remaining brine in the adjacent matrix blocks will flow into the fractures through capillary flow for drying until the brine saturation in the matrix reaches irreducible brine saturation. The irreducible brine in the rock matrix is then vaporized to dryness, precipitating salt into the rock matrix. Thus, the saturation of salt in the fractures comes from the remaining brine after drainage.

Reduction in the flow radii of the capillary tubes after salt deposition can be estimated from[41]

$$\Delta r_i = \frac{2}{3} \frac{S_{si} r_i}{l_{di}} \quad (18)$$

After calculating $\Delta r_i$, the impact of the deposited salt in the matrix block can be computed.

**2.6. Simulation Procedure and Data.** The objective of the simulation is to estimate change in absolute permeability and porosity based on salt distribution after complete dry-out during $CO_2$ injection into dual-porosity rocks. Since this is a static model, the interest is in quantifying the storage potential before and after salt deposition. The amount and distribution of precipitated salt in the rock are modeled based on assumptions derived from previous experimental findings. The general simulation procedure is as follows:

1. The initial rock permeability, $k_i$, and porosity, $\phi_i$, are computed from eqs 1, 2, 12, 13, 16, or 17 based on the type of fractured reservoir, the number of fractures, and the fracture geometry.
2. At complete dry-out, the solid salt saturation in each region of the rock, $S_{si}$, is calculated from eq 4.
3. The effect of deposited salt on the flow areas of the fracture and rock matrix, $\Delta w_{fi}$ and $\Delta r_i$, are estimated from eqs 5 and 18, respectively, based on the type of fractured reservoir under consideration.
4. The final rock permeability and porosity after salt precipitation is then computed from eqs 8 and 9, respectively.
5. Finally, the effect of salt precipitation on $CO_2$ injectivity and storage capacity is estimated from eqs 10 and 11, respectively.

Since the objective is to investigate impairment around the wellbore injection inlet, a core-scale Berea sandstone block is considered. The block of length 20 cm has a width of 6.015 cm and a height of 4 cm. With an average fracture density of 50 $m^{-1}$, the reservoir rock contains five fractures of widths $w_{f1}$ = 10 $\mu$m, $w_{f2}$ = 40 $\mu$m, $w_{f3}$ = 20 $\mu$m, $w_{f4}$ = 50 $\mu$m, and $w_{f5}$ = 30 $\mu$m and heights $h_{f1}$ = 2.0 cm, $h_{f2}$ = 1.0 cm, $h_{f3}$ = 1.5 cm, $h_{f4}$ = 1.8 cm, and $h_{f5}$ = 1.2 cm, interspersed between rock matrix blocks of dimensions $l$ = 20 cm, $w$ = 2 cm, and $h$ = 4 cm. We assume that the fractures run through the entire length of the rock. The rock has a porosity of 20% and an irreducible brine saturation of 0.2.[13] The wetting phase is a NaCl brine with brine salinity from 50 to 200 g/L. A summary of data used in the simulation is presented in Table 1. Other specific data used in the various studies will be presented with the results.

**Table 1. Summary of General Data Used in the Simulation**

| data | value | units |
|---|---|---|
| block dimensions | 0.2 × 0.06015 × 0.04 | m |
| $l_{d1}$ | 0.1 | |
| $l_{d2}$ | 0.45 | |
| $l_{d3}$ | 0.85 | |
| $\alpha$ | 2 | |
| $S_{wr}$ | 0.2 | |
| $\rho_{salt}$ | 2160 | g/L |
| $r_c$ | $3 \times 10^{-6}$ | m |
| $\phi_m$ | 20 | % |

## 3. RESULTS

Results of the studies are presented in this section. First, the simulation conditions are outlined, followed by a description of the results. The basic mechanisms are described, and the underlying parameters are identified. Some limitations of the modeling process are also presented.

**3.1. Type I Fractured Reservoirs.** The reservoir rock is filled with NaCl brine of specific initial concentration prior to $CO_2$ injection. Dry supercritical $CO_2$ is injected into the reservoir rock at a constant rate to vaporize brine and precipitate salt into the fractures. The deposited salt reduces the fracture aperture and impairs flow and $CO_2$ storage capacity. The current model is only a static model capable of quantifying the permeability and porosity change based on salt distribution in the fractures and rock matrix at complete dry-out of the reservoir rock. Since the fractures or macropores are the main source of fluid conductivity in type I reservoirs, the matrix blocks only supply brine to the adjacent fractures through capillary flow.

*3.1.1. Effect of Salt Precipitation on Injectivity and Storage Capacity.* Figure 3a,b shows injectivity impairment and

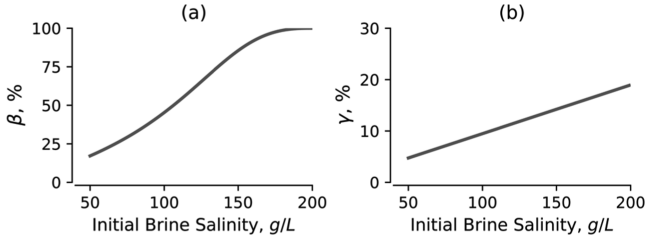


**Figure 3.** Effect of salt precipitation on (a) $CO_2$ injectivity and (b) storage capacity during $CO_2$ injection into fractured reservoirs.


https://dx.doi.org/10.1021/acsomega.0c01687
ACS Omega 2020, 5, 14776−14785

reduction of storage capacity induced by salt precipitation at varying initial brine salinities, respectively. $CO_2$ injectivity impairment increased when initial brine salinity was increased from 50 to 200 g/L (Figure 3a). At complete dry-out, the amount of salt dropped out in the fractures increases with initial salinity of the resident brine. High solid salt saturation in the fractures decreases the fracture aperture and the flow area available for $CO_2$ flow. Figure 3a also shows that the flow inlet of the rock could be completely plugged with salt at a brine salinity of about 180 g/L. Similarly, reduction in storage capacity increases slightly with brine salinity (Figure 3b).

From Figure 3, it can be deduced that the effect of salt precipitation on injectivity is almost fourfold higher than the effect on $CO_2$ storage capacity. Due to the high fluxes, drying and salt precipitation commence at the injection inlet where the solid salt saturation is highest in region $L_1$. Thus, the injection inlet is quickly clogged by salt while the downstream sections of the fracture remain open or slightly impaired. Therefore, the flow area is reduced significantly at the injection inlet, while the downstream sections of the fractures remain open for $CO_2$ storage. This explains why salt precipitation affects injectivity more compared to the volumetric storage space.

*3.1.2. Effect of Irreducible Brine Saturation.* Rocks with varying irreducible brine saturation were simulated to evaluate the influence of irreducible brine saturation in the rock matrix on the amount of salt precipitated in the fractures and the consequences on porosity and permeability of the reservoir rock. Three sandstone rocks with approximate irreducible brine saturation values of 0.1, 0.2, and 0.3 were tested.

From Figure 4, $CO_2$ injectivity impairment decreased when irreducible brine in the rock matrix increased stepwise from 0.1

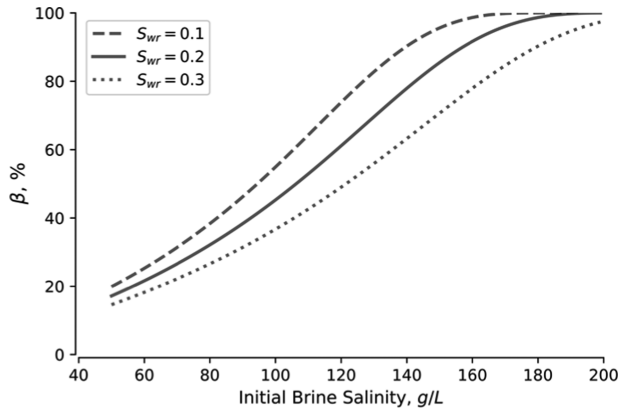


**Figure 4.** Effect of immobile brine saturation in the matrix blocks on the amount of salt precipitated in the fractures and $CO_2$ injectivity.

to 0.3. In type I reservoirs, the irreducible brine saturation in the adjacent matrix blocks affects the amount of brine supplied to the fractures for drying and salt precipitation. Rocks with high irreducible brine saturation retain more brine and release less brine into the fractures for vaporization. This reduces the solid salt saturation in the fractures after salt precipitation and consequently decreases $CO_2$ injectivity impairment. Figure 4 also shows that rocks with low irreducible brine saturation will attain complete injectivity loss at lower brine salinity compared to rocks with high irreducible brine saturation. Thus, at the same initial brine saturation, more salt is precipitated in the fractures of rocks with lower irreducible brine saturation.

*3.1.3. Effect of Fracture Geometry.* Rectangular- and elliptical-shaped fractures were simulated to evaluate the influence of fracture geometry on $CO_2$ injectivity and storage capacity. The results of the simulation are shown in Figure 5.

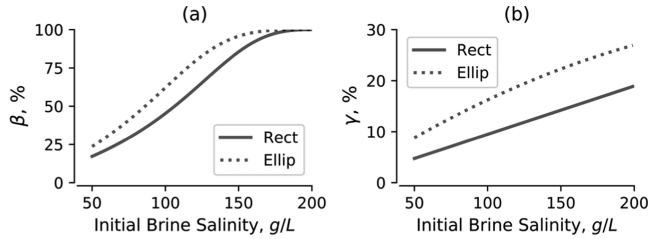


**Figure 5.** Effect of fracture geometry on salt precipitation and the consequences on (a) $CO_2$ injectivity and (b) storage capacity in fractured sandstone reservoirs.

Figure 5a shows that for the same initial saturating brine salinity, $CO_2$ injectivity impairment is higher in the elliptical fractures compared to the rectangular fractures. Since the precipitated salt is deposited along the walls of the fractures, injectivity impairment depends mainly on the effect of deposited salt on the fracture aperture. The elliptical fractures have narrower aperture along the cross section compared to the rectangular fractures. Thus, salt deposition reduces the space available for $CO_2$ flow more in the elliptical fractures compared to the rectangular-shaped fractures, which have a wider aperture (Figure 6).

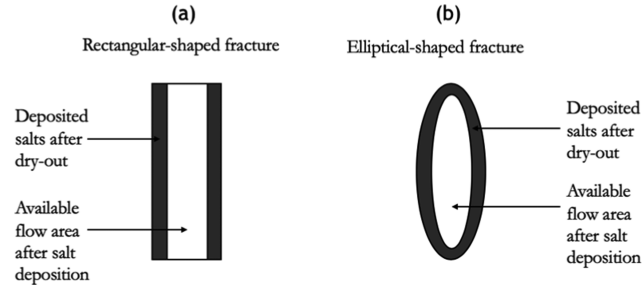


**Figure 6.** Schematics of the aperture cross section of (a) rectangular-shaped fractures and (b) elliptical-shaped fractures after complete dryness and salt precipitation.

Fracture geometry also affects $CO_2$ storage capacity (Figure 5b). The elliptical fractures are plugged up by salt faster at the injection inlet compared to the rectangular-shaped fractures due to their narrow width. After the fracture inlets are plugged with salt, the remaining sections of the fractures downstream still contain some spaces for $CO_2$ storage as solid salt saturation reduces gradually downstream. The rectangular fractures have more open spaces with higher storage capacity even after salt precipitation at the injection inlet. The fractures continue to conduct $CO_2$. Thus, $CO_2$ injectivity and storage capacity are impaired more severely in the elliptical fractures due to the high flow resistance at the injection inlet and generally less space available for $CO_2$ storage in the remaining sections of the fractures.

**3.2. Type II Fractured Reservoirs.** In type II fractured reservoirs, $CO_2$ injectivity and volumetric storage capacity are contributed by the fractures and the matrix blocks. To study the effect of salt precipitation on storage potential in type II fractured reservoirs, the reservoir rock was initially saturated


https://dx.doi.org/10.1021/acsomega.0c01687
ACS Omega 2020, 5, 14776−14785

fully with NaCl brine. The rock was then flooded with supercritical $CO_2$ at a constant injection rate. The injected $CO_2$ invades the fractures first before the rock matrix in order of low flow resistance. We assume that all of the brine in the fractures is swept out during immiscible $CO_2$−brine displacement. Figure 7 shows the pressure drop profiles measured during

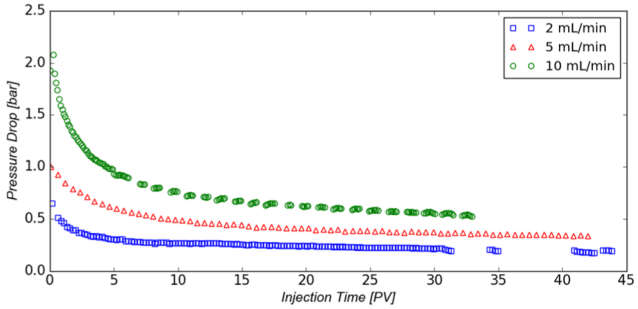


**Figure 7.** Pressure drop profile for $CO_2$ injection into Berea sandstone core initially saturated with formation water.

$CO_2$ injection into a Berea sandstone core at various injection flow rates.[42] The pressure drop profiles show that almost half of the initial saturating brine is swept out of the core after about 5 pore volumes (PV) of supercritical $CO_2$ injection. Based on this insight, we assume a mobile brine saturation of 0.6 in the matrix blocks. We also assume that $CO_2$ will immiscibly displace all mobile brine out of the matrix blocks as effluent. This gives a remaining brine saturation of 0.4. Since the rock has an irreducible brine saturation of 0.2, this leaves a brine saturation of 0.2 to be supplied to the fractures through capillary flow. The immobile brine saturation of 0.2 is then vaporized by injected $CO_2$ to dryness, precipitating salt into the rock matrix.

The effects of salt drop-out on $CO_2$ injectivity and storage volume in type I and type II fractured reservoirs are compared in Figure 8. Figure 8a shows that $CO_2$ injectivity impairment was

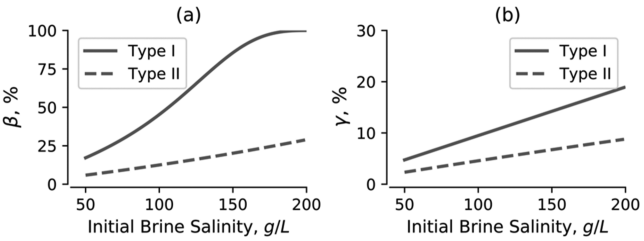


**Figure 8.** Comparison of the effects of salt precipitation on (a) well injectivity and (b) $CO_2$ storage capacity in type I and type II fractured reservoirs.

significantly higher in type I reservoirs compared to type II reservoirs. In type I reservoirs, only brine in the fractures is swept out as effluent during immiscible displacement. In type II reservoirs, the mobile brine in the rock matrix is also swept out as effluent in addition to all of the brine in the fractures during immiscible displacement. Thus, less amount of brine is retained in the rock for drying and salt precipitation in the type II fractured reservoir. Also, in type II reservoirs, both the fractures and rock matrix contribute to $CO_2$ injectivity, whereas in type I reservoirs, only the fractures contribute to $CO_2$ injectivity. In addition, the solid salt saturation in the fractures in type II reservoirs will be lower compared to type I reservoirs.

Figure 8b shows that volumetric storage capacity was also reduced less in type II reservoirs compared to type I reservoirs. With the same initial brine salinity, type II reservoirs will have lower solid salt saturation in the fractures at dry-out. In addition, the rock matrix also contributes to $CO_2$ storage in type II reservoirs since only immobile brine is vaporized in the rock matrix. On the contrary, in type I reservoirs, $CO_2$ storage is controlled mainly by the fractures where salt precipitation is also comparatively higher.

## 4. DISCUSSION AND PRACTICAL IMPLICATIONS

Most of the hydrocarbon-bearing rocks in the world are naturally fractured reservoirs, which can be converted for $CO_2$ storage.[39] Deep saline aquifers have large volumetric storage potential and accessibility. Therefore, fractured deep saline reservoirs offer a valuable option for $CO_2$ storage. However, salt precipitation in the wellbore inlet could threaten $CO_2$ storage in saline reservoirs. Salt precipitation in fractured reservoirs is unique and therefore requires special investigation. In the present work, a static core-scale analytical model has been developed based on previous experimental findings to investigate the quantitative impact of salt deposition on $CO_2$ storage potential in dual-porosity rocks. The objective is to quantify the impact of salt deposition on $CO_2$ injectivity and volumetric storage capacity in fractured deep saline reservoirs.

Two types of fractured reservoirs were considered: type I and type II fractured reservoirs. In type I fractured reservoirs, storage capacity and well injectivity are contributed mainly by the fractures or macropores with the adjacent matrix blocks or micropores supplying brine to the fractures through capillary flow. In type II reservoirs, both the fractures and the adjacent matrix blocks contribute to $CO_2$ storage capacity and injectivity. Two types of fracture geometry, rectangular and elliptical fractures, were investigated. The rock was initially filled with NaCl brine with specific brine salinity, and dry supercritical $CO_2$ was injected into the block to displace and dry out the brine. The impact of salt precipitation was then modeled based on the expected amount and distribution of salt saturation in the rock. Brine salinity between 50 and 200 g/L was considered.

A 1D static model based on the Warren−Root framework was used in the simulation process. Only the physical mechanisms of salt deposition and its consequences on injectivity were considered. Furthermore, a homogeneous saline reservoir was assumed, where salt precipitation is severe around the wellbore injection region, where fluxes are highest. It was also assumed that prior to drying and salt precipitation, all brine in the fractures along the flow direction is displaced out of the fractures by immiscible $CO_2$−brine flow. Thus, only brine supplied by the adjacent matrix blocks is dried in the fractures. Although these simplified assumptions limit the application of the work, the findings do not compromise on the main mechanisms of $CO_2$ flow around the injection vicinity, which is the main interest of this work. The results are therefore practically valuable and provide useful understanding of drying and the effect of salt deposition in fractured saline reservoirs.

Generally, salt precipitation had a higher impact on $CO_2$ injectivity compared to storage capacity. $CO_2$ injectivity impairment and storage capacity reduction both increased with initial saturating brine salinity. However, for the same initial brine salinity, injectivity was impaired about fourfold compared to storage capacity even in type I fractured reservoirs. Ott et al.[13] reported that because of solute transport between the pores through capillary flow after drainage, the accumulated salt


https://dx.doi.org/10.1021/acsomega.0c01687
ACS Omega 2020, 5, 14776−14785

around the injection inlet is more than the original salt concentration in the brine. Due to the high fluxes, a saturation gradient is quickly created between the injection inlet and the rest of the rock, which draws brine toward the injection inlet for drying and eventual salt precipitation. Thus, the injection inlet is quickly plugged by precipitated salt. Therefore, while the injection inlet is clogged by salt, the remaining sections of the rock still contain open spaces for $CO_2$ storage. While the rock might not easily conduct $CO_2$ at the inlet even in the fractures, it has open spaces downstream in the reservoir for $CO_2$ storage. This is probably why salt precipitation affects injectivity more significantly compared to the volumetric storage space in the rock.

The amount of entrapped brine in the matrix blocks after drainage was found to contribute significantly to the solid salt saturation in the fractures in type I reservoirs. The injected $CO_2$ invades the fractures first because of the low entry pressure.[38] Therefore, the fractures are quickly drained. A saturation gradient is then created between the fractures and the matrix block that draws brine into the fractures through capillary flow. The amount of brine supplied to the fractures depends on the immobile brine saturation in the rock matrix. Rocks with low immobile brine saturation would supply more brine to the fractures for drying and eventual salt precipitation. Therefore, while March et al.[39] have shown by numerical simulations the viability of fractured reservoirs for $CO_2$ storage, we submit that not all types of fractured reservoirs may have the requisite injectivity for $CO_2$ storage. Type I fractured deep saline reservoirs that entrap a low amount of brine in the matrix blocks may not be suitable for $CO_2$ storage due to the high potential for salt precipitation in the fractures.

The geometry of the fracture aperture may also affect the impact of salt precipitation on $CO_2$ storage potential. The impact of salt precipitation was generally higher for fractures with elliptical aperture compared to fractures with rectangular cross section. Fractures with elliptical cross section have narrower aperture after salt precipitation. Therefore, the flow area in elliptical fractures is severely reduced since the precipitated salt is mostly deposited along the walls of the fractures. On the other hand, fractures with rectangular cross section have more open width and therefore are less susceptible to salt plugging.

Generally, salt precipitation had less impact on $CO_2$ storage capacity and well injectivity in type II fractured reservoirs compared to type I fractured reservoirs. In type II reservoirs, almost all of the mobile brine is displaced out of the rock through immiscible $CO_2$−brine displacement, leaving less entrapped brine in the matrix blocks to be supplied to the fractures for drying. Thus, type II fractured reservoirs retain less amount of brine for vaporization and eventual salt precipitation. In addition, the rock matrix contributes significantly to $CO_2$ storage and injectivity in type II reservoirs because only the irreducible brine is dried in the matrix blocks. This is consistent with the experimental findings by Ott et al.[13] who reported that salt coming from the matrix blocks is only precipitated in the fractures with no precipitation at all observed in the matrix blocks. These properties suggest that type II fractured deep saline reservoirs could be more suitable for $CO_2$ storage compared to type I reservoirs.

Ott et al.[13] have also reported that the ratio of macropores to micropores determines the effect of salt precipitation on the effective permeability in dual-porosity rocks. However, we have found that the conductivity of the matrix blocks could have a major impact on the amount of salt deposited in the fractures and $CO_2$ injectivity. If the matrix blocks are highly conductive, they retain less brine after drainage and therefore supply less amount of brine to the fractures for drying and eventual precipitation.

Generally, salt precipitation is a serious threat to $CO_2$ storage, especially in fractured deep saline reservoirs, where the saturating brine salinity is high. We have reported interesting findings based on static dual-porosity models that were used to quantify the effect of deposited salt on $CO_2$ injectivity in fractured rocks at complete dryness. Based on the insight gained, we observe that type I fractured deep saline reservoirs may only be suitable for $CO_2$ storage if the fracture density is very high and brine salinity is very low due to their high susceptibility to salt clogging at the injection inlet. However, type II fractured deep saline reservoirs could offer strong potential for $CO_2$ storage as they are less affected by salt precipitation. Although the present findings are mainly based on simplified static analytical models, the insight gained provide valuable understanding of the mechanisms of salt deposition in naturally fractured deep saline reservoirs. The findings also serve a strong foundation upon which a dynamic model may be developed to improve the understanding of some of the mechanisms.

## 5. CONCLUSIONS

A $CO_2$ storage prospect must have adequate storage potential to receive $CO_2$ at sustainable injection rates and hold large volumes of the injected gas. Deep saline aquifers offer the best option in terms of storage capacity. However, a significant number of deep saline reservoirs are naturally fractured. Drying and salt precipitation during $CO_2$ injection may pose a threat to the potential of saline reservoirs for $CO_2$ storage. Although naturally fractured deep saline reservoirs could be potential candidates for $CO_2$ storage, they are among the prospects yet to receive deserved research attention.

We developed analytical models to quantify the impact of salt precipitation on $CO_2$ storage potential during $CO_2$ injection into fractured deep saline reservoirs. Two types of fractured saline reservoirs were considered; type I fractured reservoirs, where storage capacity and injectivity are contributed by only fractures with the adjacent matrix blocks acting as brine reservoirs that supply brine to the fractures, and type II fractured reservoirs, where both fractures and the adjacent matrix blocks contribute to $CO_2$ storage and injectivity. The effects of some underlying parameters such as immobile brine saturation and fracture geometry were also investigated. Some of the main findings of the work are summarized as follows:

1. Salt precipitation was found to have an about fourfold impact on $CO_2$ injectivity compared to the volumetric storage capacity. Drying commences at the injection inlet and precipitated salt plugs the fracture inlets, leaving the remaining sections of the fractures downstream with spaces available for $CO_2$ storage. Thus, the fractures are unable to conduct $CO_2$ to fill in the spaces behind the clogged region.
2. Contrary to previous reports, we found that not all fractured saline reservoirs may be suitable for $CO_2$ storage. Type II fractured saline reservoirs were found to be more suitable for $CO_2$ storage due to the low impact of salt precipitation on injectivity. The matrix blocks retain less brine after drainage and therefore supplies less brine to the fractures for salt precipitation. In addition, the


https://dx.doi.org/10.1021/acsomega.0c01687
ACS Omega 2020, 5, 14776−14785

matrix blocks conduct $CO_2$ and contribute significantly to injectivity and storage capacity.

3. Fractures in saline reservoirs with high immobile brine saturation in the rock matrix after drainage are more susceptible to salt clogging. The entrapped brine in the rock matrix after immiscible displacement influences the amount of brine supplied to the fractures during vaporization. Fractured rocks, where the rock matrix retains more brine, supply a high amount of brine to the fractures for salt precipitation.
4. Fractures with a rectangular aperture were less likely to be clogged by salt compared to fractures with an elliptical aperture. Rectangular fractures have more open apertures after salt precipitation compared to elliptical fractures.

Although these findings are based on simplified static core-scale analytical models, they offer valuable understanding of how salt precipitation affects $CO_2$ storage potential in fractured saline reservoirs. The results also serve as a strong foundation upon which a dynamic model may be developed to investigate the mechanisms and impact of underlying parameters.

## AUTHOR INFORMATION


### Corresponding Author

**Yen A. Sokama-Neuyam** − *Department of Petroleum Engineering, Kwame Nkrumah University of Science and Technology, Kumasi 00233, Ghana;* orcid.org/0000-0002-3402-0099

### Authors

**Patrick Boakye** − *Department of Chemical Engineering, Kwame Nkrumah University of Science and Technology, Kumasi, Ghana*

**Wilberforce N. Aggrey** − *Department of Petroleum Engineering, Kwame Nkrumah University of Science and Technology, Kumasi 00233, Ghana*

**Nicholas O. Obeng** − *Department of Petroleum Engineering, Kwame Nkrumah University of Science and Technology, Kumasi 00233, Ghana*

**Francis Adu-Boahene** − *Department of Chemical Engineering, Kwame Nkrumah University of Science and Technology, Kumasi, Ghana*

**Seung Han Woo** − *Department of Chemical and Biological Engineering, Hanbat National University San 16-1, Daejeon 34158, Republic of Korea;* orcid.org/0000-0001-8250-973X

**Jann Rune Ursin** − *Department of Energy and Petroleum Engineering, University of Stavanger, Stavanger 4036, Norway*

Complete contact information is available at: https://pubs.acs.org/10.1021/acsomega.0c01687


### Notes

The authors declare no competing financial interest.

## ACKNOWLEDGMENTS

The authors thank Prof. Kwabena B. Nyarko, Head of Department, Petroleum Engineering Department of Kwame Nkrumah University of Science and Technology (KNUST), for his support and encouragement. Special appreciation is also extended to College of Engineering, KNUST.

## REFERENCES


(1) IEA. Global Energy & CO2 Status Report: Emissions, 2019. https://www.iea.org/geco/emissions/.

(2) Miri, R. *Effects of $CO_2$-Brine-Rock Interactions on $CO_2$ Injectivity—Implications for CCS*; University of Oslo, 2015.

(3) Zhao, X.; Liao, X.; Wang, W.; Chen, C.; Rui, Z.; Wang, H. The $CO_2$ storage capacity evaluation: Methodology and determination of key factors. *J. Energy Inst.* **2014**, *87*, 297−305.

(4) Zhao, X.; Rui, Z.; Liao, X. Case studies on the $CO_2$ storage and EOR in heterogeneous, highly water-saturated, and extra-low permeability Chinese reservoirs. *J. Nat. Gas Sci. Eng.* **2016**, *29*, 275−283.

(5) Zhao, X. L.; Liao, X. W.; Wang, W. F.; Chen, C. Z.; Liao, C. L.; Rui, Z. H. Estimation of $CO_2$ storage capacity in oil reservoir after waterflooding: Case studies in Xinjiang oilfield from West China. *Adv. Mater. Res.* **2013**, *734*−*737*, 1183−1188.

(6) Jiang, J.; Rui, Z.; Hazlett, R.; Lu, J. An integrated technical-economic model for evaluating $CO_2$ enhanced oil recovery development. *Appl. Energy* **2019**, *247*, 190−211.

(7) Cui, G.; Wang, Y.; Rui, Z.; Chen, B.; Ren, S.; Zhang, L. Assessing the combined influence of fluid-rock interactions on reservoir properties and injectivity during $CO_2$ storage in saline aquifers. *Energy* **2018**, *155*, 281−296.

(8) Cui, G.; Ren, S.; Rui, Z.; Ezekiel, J.; Zhang, L.; Wang, H. The influence of complicated fluid-rock interactions on the geothermal exploitation in the $CO_2$ plume geothermal system. *Appl. Energy* **2018**, *227*, 49−63.

(9) Borgia, A.; Pruess, K.; Kneafsey, T. J.; Oldenburg, C. M.; Pan, L. Simulation of $CO_2$-EGS in a fractured reservoir with salt precipitation. *Energy Procedia* **2013**, *37*, 6617−6624.

(10) Borgia, A.; Pruess, K.; Kneafsey, T. J.; Oldenburg, C. M.; Pan, L. Numerical simulation of salt precipitation in the fractures of a $CO_2$-enhanced geothermal system. *Geothermics* **2012**, *44*, 13−22.

(11) Baines, S. J.; Worden, R. H.; Jackson, R. E. *Geological Storage of Carbon Dioxide*; Special Publications: London, 2009; Vol. *233*, pp 115−116.

(12) Gunter, W. D.; Wong, S.; Cheel, D. B.; Sjostrom, G. Large $CO_2$ sinks: Their role in the mitigation of greenhouse gases from an international, national (Canadian) and provincial (Alberta) perspective. *Appl. Energy* **1998**, *61*, 209−227.

(13) Ott, H.; Snippe, J.; de Kloe, K.; Husain, H.; Abri, A. Salt precipitation due to sc-gas injection: Single versus multi-porosity rocks. *Energy Procedia* **2013**, *37*, 3319−3330.

(14) Peysson, Y.; André, L.; Azaroual, M. Well injectivity during $CO_2$ storage operations in deep saline aquifers-Part 1: Experimental investigation of drying effects, salt precipitation and capillary forces. *Int. J. Greenhouse Gas Control* **2014**, *22*, 291−300.

(15) André, L.; Peysson, Y.; Azaroual, M. Well injectivity during $CO_2$ storage operations in deep saline aquifers − Part 2: Numerical simulations of drying, salt deposit mechanisms and role of capillary forces. *Int. J. Greenhouse Gas Control* **2014**, *22*, 301−312.

(16) Bacci, G.; Korre, A.; Durucan, S. Experimental investigation into salt precipitation during $CO_2$ injection in saline aquifers. *Energy Procedia* **2011**, *4*, 4450−4456.

(17) Pruess, K.; Muller, N. Formation dry-out from $CO_2$ injection into saline aquifers: 1. effects of solids precipitation and their mitigation. *Water Resour. Res.* **2009**, *45*, 1−11.

(18) Ott, H.; Roels, S. M.; Kloe, K. De. Salt precipitation due to supercritical gas injection: I. Capillary-driven flow in unimodal sandstone. *Int. J. Greenhouse Gas Control* **2015**, *43*, 247−255.

(19) Zuluaga, E.; Muñoz, N. I.; Obando, G. In *An Experimental Study to Evaluate Water Vaporisation and Formation Damage Caused by Dry Gas Flow Through Porous Media*, International Symposium on Oilfield Scale; Society of Petroleum Engineers, 2001.

(20) Pruess, K. Formation dry-out from $CO_2$ injection into saline aquifers: 2. analytical model for salt precipitation. *Water Resour. Res.* **2009**, *45*, 1−6.

(21) Mahadevan, J.; Sharma, M. M.; Yortsos, Y. C.; Mahadevan, J.; Sharma, M. M.; Yortsos, Y. C. Water removal from porous media by gas injection: Experiments and simulation. *Transp. Porous Media* **2007**, *66*, 287−309.




https://dx.doi.org/10.1021/acsomega.0c01687
*ACS Omega* 2020, 5, 14776−14785

(22) Roels, S. M.; Ott, H.; Zitha, P. L. J. $\mu$-CT analysis and numerical simulation of drying effects of $CO_2$ injection into brine-saturated porous media. *Int. J. Greenhouse Gas Control* **2014**, *27*, 146−154.
(23) Muller, N.; Qi, R.; Mackie, E.; Pruess, K.; Blunt, M. J. $CO_2$ injection impairment due to halite precipitation. *Energy Procedia* **2009**, *1*, 3507−3514.
(24) Wang, Y.; Mackie, E.; Rohan, J.; Luce, T.; Knabe, R.; Appel, M. *Experimental Study on Halite Precipitation during $CO_2$ Sequestration*; International Symposium of the Society of Core Analysts: Noordwijk, The Netherlands, 2009; pp 1−12.
(25) Tang, Y.; Yang, R.; Du, Z.; Zeng, F. Experimental study of formation damage caused by complete water vaporization and salt precipitation in sandstone reservoirs. *Transp. Porous Media* **2015**, *107*, 205−218.
(26) Bacci, G.; Durucan, S.; Korre, A. Experimental and Numerical Study of the Effects of Halite Scaling on Injectivity and Seal Performance During $CO_2$ Injection in Saline Aquifers. *Energy Procedia* **2013**, *37*, 3275−3282.
(27) Kim, M.; Sell, A.; Sinton, D. Aquifer-on-a-Chip: understanding pore-scale salt precipitation dynamics during $CO_2$ sequestration. *Lab Chip* **2013**, *13*, 2508−2518.
(28) Giorgis, T.; Carpita, M.; Battistelli, A. 2D modeling of salt precipitation during the injection of dry $CO_2$ in a depleted gas reservoir. *Energy Convers. Manage.* **2007**, *48*, 1816−1826.
(29) Hurter, S.; Berge, J.; Labregere, D. Simulations for CO2 injection projects with Compositional Simulator. *Offshore Eur.* **2007**, 4−7.
(30) Zeidouni, M.; Pooladi-Darvish, M.; Keith, D. Analytical solution to evaluate salt precipitation during $CO_2$ injection in saline aquifers. *Int. J. Greenhouse Gas Control* **2009**, *3*, 600−611.
(31) Van Golf-Racht, T. B. D. T. Fundamentals of Fractured Reservoir Engineering. In *Developments in Petroleum Science*; Elsevier, 1982; Vol. *12*, pp 299−351.
(32) Tiab, D.; Donaldson, E. C. *Naturally Fractured Reservoirs*; Gulf Professional Publishing: Boston, 2016; Chapter 8, pp 415−481.
(33) Oh, J.; Kim, K. Y.; Han, W. S.; Kim, T.; Kim, J. C.; Park, E. Experimental and numerical study on supercritical $CO_2$/brine transport in a fractured rock: Implications of mass transfer, capillary pressure and storage capacity. *Adv. Water Resour.* **2013**, *62*, 442−453.
(34) Tian, Z.; Xing, H.; Tan, Y.; Gu, S.; Golding, S. D. Reactive transport LBM model for $CO_2$ injection in fractured reservoirs. *Comput. Geosci.* **2016**, *86*, 15−22.
(35) Rezk, M. G.; Foroozesh, J. Study of Convective-Diffusive Flow during $CO_2$ Sequestration in Fractured Heterogeneous Saline Aquifers. *J. Nat. Gas Sci. Eng.* **2019**, *69*, No. 102926.
(36) Ahmed, R.; Li, J. A numerical framework for two-phase flow of $CO_2$ injection into the fractured water-saturated reservoirs. *Adv. Water Resour.* **2019**, *130*, 283−299.
(37) Ding, M.; Gao, M.; Wang, Y.; Qu, Z.; Chen, X. Experimental study on $CO_2$ -EOR in fractured reservoirs: Influence of fracture density, miscibility and production scheme. *J. Pet. Sci. Eng.* **2019**, *174*, 476−485.
(38) Ott, H.; Andrew, M.; Snippe, J.; Blunt, M. J. Microscale solute transport and precipitation in complex rock during drying. *Geophys. Res. Lett.* **2014**, *41*, 8369−8376.
(39) March, R.; Doster, F.; Geiger, S. Assessment of CO2 Storage Potential in Naturally Fractured Reservoirs With Dual-Porosity Models. *Water Resour. Res.* **2018**, *54*, 1650−1669.
(40) Zhao, R.; Cheng, J. Effects of temperature on salt precipitation due to formation dry-out during $CO_2$ injection in saline aquifers. *Greenhouse Gases Sci. Technol.* **2017**, *7*, 624−636.
(41) Sokama-Neuyam, Y. A.; Ursin, J. R. The coupled effect of salt precipitation and fines mobilization on $CO_2$ injectivity in sandstone. *Greenhouse Gases Sci. Technol.* **2018**, *8*, 1066−1078.
(42) Sokama-Neuyam, Y. A.; Ginting, P. U. R.; Timilsina, B.; Ursin, J. R. The impact of fines mobilization on $CO_2$ injectivity: An experimental study. *Int. J. Greenhouse Gas Control* **2017**, 65.


https://dx.doi.org/10.1021/acsomega.0c01687
*ACS Omega* 2020, 5, 14776−14785